How a Small Reef in the Kuroshio Cultivates the Ocean

Hasegawa, Daisuke
Fisheries Resources Institute, Japan Fisheries Research and Education Agency (FRA)

Matsuno, Takeshi
Research Institute for Applied Mechanics, Kyushu University

Tsutsumi, Eisuke
Atmosphere and Ocean Research Institute, The University of Tokyo

千手, 智晴
Research Institute for Applied Mechanics, Kyushu University

他

出版情報：Geophysical Research Letters. 48 (7), pp.e2020GL092063-, 2021-03-25. American Geophysical Union
バージョン：

Geophysical Research Letters

RESEARCH LETTER
10.1029/2020GL092063

How a Small Reef in the Kuroshio Cultivates the Ocean

D. Hasegawa[1], T. Matsuno[2], E. Tsutsumi[3], T. Senjyu[2], T. Endoh[2], T. Tanaka[1], N. Yoshie[4], H. Nakamura[5], A. Nishina[5], T. Kobari[5], T. Nagai[6], and X. Guo[4]

[1]Fisheries Resources Institute, Japan Fisheries Research and Education Agency (FRA), Shiogama, Japan, [2]Research Institute for Applied Mechanics, Kyushu University, Kasuga, Japan, [3]Atmosphere and Ocean Research Institute, The University of Tokyo, Kashiwa, Japan, [4]Center for Marine Environmental Studies, Ehime University, Matsuyama, Japan, [5]Faculty of Fisheries, Kagoshima University, Kagoshima, Japan, [6]Department of Ocean Sciences, Tokyo University of Marine Science and Technology, Tokyo, Japan

Key Points:

- Flow separations and trains of Kelvin-Helmholtz billows mix the water column around a small reef in the Kuroshio
- Doming of isopycnals/nitraclines suggests strong upwelling in the lee of the reef
- Turbulent nitrate fluxes reach up to $O(10^3$ mmol m^{-2} day$^{-1})$

Correspondence to:
D. Hasegawa,
daisukeh@affrc.go.jp

Citation:
Hasegawa, D., Matsuno, T., Tsutsumi, E., Senjyu, T., Endoh, T., Tanaka, T., et al. (2021). How a small reef in the Kuroshio cultivates the ocean. *Geophysical Research Letters*, *48*, e2020GL092063. https://doi.org/10.1029/2020GL092063

Received 14 DEC 2020
Accepted 25 FEB 2021

Abstract Vertical nitrate fluxes associated with turbulent mixing and upwelling around a small reef in the Kuroshio are quantified by continuously deploying a turbulence microstructure profiler with an attached submersible ultraviolet nitrate analyzer while drifting from the upstream to the downstream of the reef. Flow separations and trains of Kelvin-Helmholtz billows (thickness = 60 m) are identified using a shipboard ADCP and an echo-sounder. The turbulence diffusivity associated with the vigorous turbulent mixing reaches up to $O(10^{-1}$ m^2 s$^{-1})$, resulting in strong nitrate fluxes of $O(1$–10^3 mmol m^{-2} day$^{-1})$. In addition, large differences between the upstream and downstream density profiles suggest a strong upwelling velocity of $O(10^{-3}$ m s$^{-1})$, as well as an upwelling nitrate flux of $O(10^2$ mmol m^{-2} day$^{-1})$ in the entire subsurface layer.

Plain Language Summary Vertical nitrate fluxes associated with flow-topography interactions around a small reef in the Kuroshio Current are quantified using state-of-the-art oceanographic instruments. When the flow passes over a shallow sill on the flank of the reef, the velocity differences between layers intensify, resulting in a substantial vertical overturning and mixing of the water column. This turbulent mixing causes the observed nitrate flux from deep water to reach a value among the highest observed worldwide.

1. Introduction

Enhanced biological production associated with flow disturbance due to island or shallow seamounts is known as the "Island Mass Effect" (IME) (Doty & Oguri, 1956). Because ridges topped by multiple small islands and seamounts are a consistent feature along the Kuroshio flow path (Hasegawa, 2019), several studies since the 1950s have reported that the Kuroshio induces IMEs (e.g., Furuya et al., 1986; Uda & Ishino, 1958, and others). However, in these earlier studies, the detailed physical processes of the IMEs were not thoroughly studied due to the complexities of the flow disturbance associated with the abrupt topographic features.

Since the reporting of extremely large upwelling velocities of $O(0.01$ m s$^{-1})$ and turbulence kinetic energy dissipation rates of $O(10^{-4}$ W kg$^{-1})$ in lees of small islands located along the Kuroshio main axis (Hasegawa et al., 2008, 2004), the ridges (I-Lan, Tokara, and Izu) over which the Kuroshio passes have been recognized as key locations for open-ocean upwelling and mixing. In recent years, multiple intensive field campaigns have been carried out with the latest observational instruments, building a quantitative understanding of the detailed physical mechanisms of flow-topography interactions in the Kuroshio Current at these ridges. For example, Chang et al. (2016) used an echo-sounder to observe 100 m-scale Kelvin-Helmholtz billows, which are structures resembling a cat's eye generated by the interaction of the Kuroshio with a seamount north of Green Island along the east coast of Taiwan. Nagai et al. (2017) developed a tow-yo-style turbulence profiling system (Underway VMP), that was used to observe layers of strong turbulence associated with bands of near-inertial wave shear excited by flow-topography interactions in the Tokara Strait. Tsutsumi et al. (2017) conducted a transect survey crossing the Kuroshio Current on the lee sides of small islands and seamounts with a turbulence microstructure profiler in order to grasp the overall distribution of turbulent vertical mixing in the Tokara Strait. Moreover, some studies have observed cold surface water formation on the lee sides of small islands in the Kuroshio and have taken these observations as evidence for the

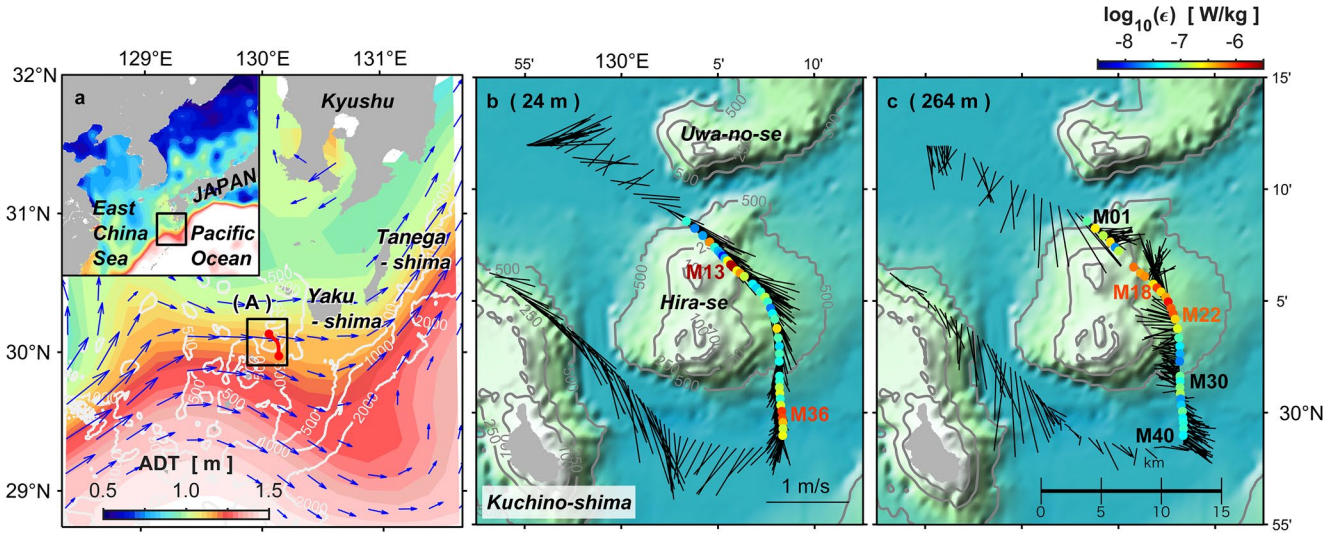

Figure 1. (a) Absolute Dynamics Topography (color scale in meters) around Tokara Strait, southwest of Kyushu, Japan, on November 16, 2016. The inset map shows the surrounding area for the study region. White lines indicate bathymetry. The blue arrows indicate the geostrophic current based on satellite altimetry, with arrows plotted only where the velocity exceeds 0.2 m s^{-1}. (b and c) Enlarged map showing bathymetry around Hira-se (the area indicated by (A) in panel (a)) with current vectors based on observations by the shipboard ADCP for depths of (b) 24 m and (c) 264 m. The colored circles indicate a depth-averaged turbulent dissipation rate in (b) the subsurface layer and (c) the intermediate layer.

occurrence of strong upwellings (e.g., Chang et al., 2019, 2013; Hsu et al., 2017, and others). Nevertheless, such upwelling studies remain somewhat descriptive given the absence of methods for directly measuring vertical velocity.

Under the OMIX project (2015–2020, Japan), interdisciplinary studies attempting to quantify the effects of turbulent mixing and upwelling caused by small islands and seamounts in the Kuroshio Current have been carried out. Nagai et al. (2019) demonstrated the enhanced turbulent vertical nitrate flux in the downstream of the Tokara Strait based on results of Underway VMP measurements with the indirectly estimated nitrate concentration using the local relationship between salinity and nitrate concentration. Hasegawa et al. (2019) developed a method for measuring the turbulent vertical nitrate flux in which an in situ nitrate sensor was attached to a turbulence profiler. Tanaka et al. (2019) used this method to demonstrate that the vertical mixing associated with rough topography at the Izu ridge elevated the nitrate flux and contributed to the nitrate component of the Kuroshio nutrient stream (Guo et al., 2013). Furthermore, Kobari et al. (2020) conducted nutrient addition experiments in oligotrophic Kuroshio water to determine the effects of turbulent nitrate flux elevation in the Tokara Strait. They found a significant increase in microzooplankton grazing on phytoplankton, suggesting that such rapid and systematic trophodynamics support biological productivity in the Kuroshio.

These remarkable scientific efforts have provided a glimpse of the spectacular Kuroshio IMEs, but some details are still missing, and therefore so is the complete picture. Herein, we focus on the detailed views of IMEs in the Kuroshio, in particular the questions of how and how much nitrate is supplied to the upper layers associated with the flow disturbance at Hira-se, a small reef in the Kuroshio.

2. Survey and Instrumentation

In November 2016, we conducted a survey using the TRV *Kagoshima Maru* (1,284 ton) around Hira-se while the northern edge of the Kuroshio was located on this reef (Figure 1a). Hira-se is the apex of an eroded conic volcano. It measures 2.5 km north-south at the surface, and it stands 500 m above its 15 km submarine foundation (Figure 1c). From 13:45 JST (GMT+9) through 23:36 JST on November 16, 2016, we passively drifted the vessel from the upstream of Hira-se with the surface current along the northern passage between Hira-se and Uwa-no-se while continuously collecting measurements of microstructure turbulence (TurboMAP-L; JFE Advantech), horizontal current (75 kHz shipboard ADCP with 16 m bin; RDI), and

echogram (EK60; Simrad) from station M01 to station M40 (refer to the colored circles in Figure 1). The shipboard wind speed was weak (average speed = 2.6 m s^{-1}) during the survey; therefore, it was assumed that the vessel drifted along the surface current.

We also observed the nitrate concentrations and the light intensities in the water column simultaneously with the deployment of the microstructure profiler to precisely quantify the turbulent vertical nitrate flux to the euphotic layer. The system observing the turbulent nitrate flux was recently developed by Hasegawa et al. (2019) and consists of a submersible nitrate sensor (Deep SUNA V2; Sea-Bird Scientific) and a PAR sensor (DEFI2-L; JFE Advantech) attached to a microstructure profiler (TurboMAP-L). The proportionality coefficient of the nitrate sensor was calibrated against the bottle-sampled nitrate profiles collected during the same cruise, and the sensor offset for each cast was determined in order to set the surface minimum value to zero (mean offset is 0.78 ± 0.22 mmol m^{-3}), since the isopycnal associated with the nitracline did not outcrop at the surface during the survey.

The vertical turbulent nitrate flux F_{NO_3} was quantified by multiplying the estimated vertical turbulent diffusivity from the microstructure measurements by the vertical gradient of the observed nitrate concentration, that is,

$$F_{NO_{3mix.}} = -K_\rho \frac{\partial NO_3}{\partial z}, \quad (1)$$

where NO_3 is the nitrate concentration.

3. Results and Discussions

3.1. Flow Perturbation and Turbulent Mixing

During the survey, the surface current was eastward upstream of Hira-se, then flowed into the channel between Uwa-no-se and Hira-se (see Figure 1b). Further, the flow in the intermediate layer (264 m, Figure 1c) was southward upstream of Hira-se, going around the shallow reefs, with some portion flowing into the channel along with the surface flow. In the channel, the surface flow turned southeast while passing over the sill extending from the northeastern edge of Hira-se. Thereafter, the surface flow turned south at the east side of Hira-se. The intermediate layer flow direction was opposite to that of the surface flow just in the lee of the sill and then oscillated between west and east downstream of the reef.

When the flow surmounted the shallow sill, the surface flow accelerated to 0.8 m s^{-1} (Figure 2a). A strong mean shear layer, namely the separated bottom boundary layer (SBBL), was evident between the surface jet and the sill peak. Profiles of microstructure shear (yellow plots in Figure 2b) indicate the development of the SBBL from the sill peak downstream, with the thickness of the turbulent layer increasing to more than 100 m by the time it reached station M15. The intensified wavy echo band in the echogram also indicates the growth of the SBBL along this trajectory (Figure 2b).

In the layer located 40 m above the seafloor at station M13 (see Figure 1b for the location), the gradient Richardson number, $Ri = N^2/S^2$, in the SBBL measured ~1 (black line in Figure 2e), which is above the critical value of 0.25, where $N^2 = -g/\rho_0\, \partial\sigma_\theta/\partial z$ is the buoyancy frequency squared, σ_θ is the potential density, ρ_0 is the reference density, g is the gravitational acceleration, and S^2 is the mean squared vertical shear. We cannot confirm the instability condition for Ri at the beginning of the SBBL close to the sill peak because the velocity data are missing due to acoustic interference at the seafloor, and the relatively coarse vertical resolution (16 m) of the velocity measurement is possibly overestimating Ri. However, the profile of the Thorpe length scale, $L_T = \sqrt{{d_T}^2}$, shows 10 m-scale thermal inversions in the SBBL (green line in Figure 2f), where d_T is the Thorpe-scale displacement. It should be noted that because the salinity quality was not sufficiently high to be used for this analysis, a temperature-based Thorpe-scale displacement d_T was used instead of a density-based value. The kinetic energy dissipation rate (ϵ; magenta line in Figure 2e) in the same depth range reaches $O(10^{-5}$ W $kg^{-1})$, and the corresponding vertical turbulent diffusivity ($K_\rho = 0.2{\cdot}\epsilon/N^2$ Osborn, 1980; blue line in Figure 2g) reaches $O(10^{-1}$ m^2 $s^{-1})$. Given the vigorous turbulent mixing and temperature inversions in the SBBL, we suspect the bottom layer in the SBBL to show the Ri value below 0.25.

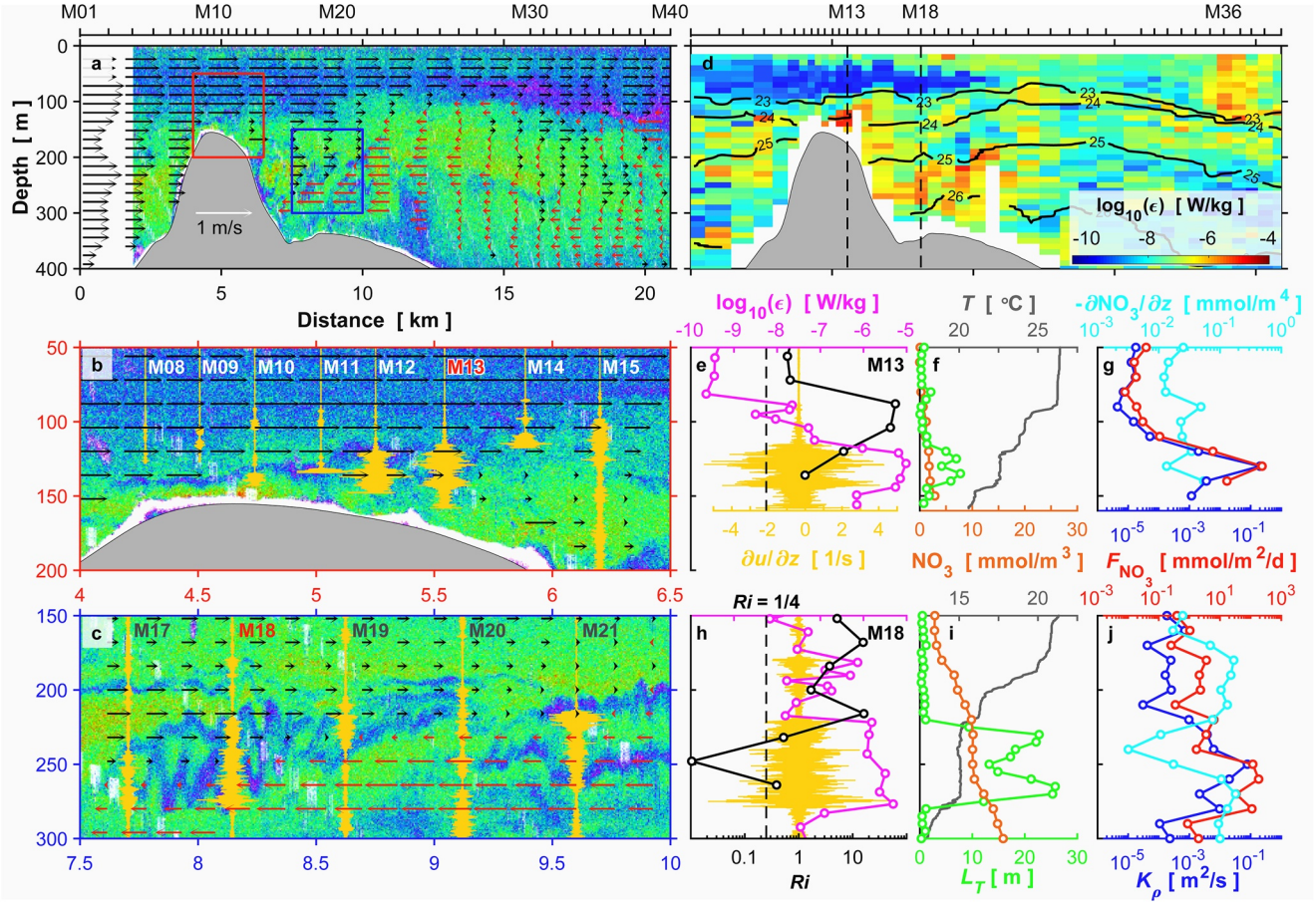

Figure 2. (a) Echogram (120 kHz) with along-stream velocity profile during the drifting survey along the flow over a sill at the northeast flank of Hira-se (see Figure 1 for the location). The red arrows indicate recirculation flow. (b and c) Detailed echograms corresponding respectively with the red and blue boxes in (a). Yellow thorny lines represent microstructure shear profiles based on observations by TurboMAP-L. (d) Vertical section of turbulent kinetic energy dissipation rate. Black contours represent isopycnals. (e–j) Vertical profiles of microstructure shear (yellow), turbulent kinetic energy dissipation rates (magenta), gradient Richardson number (*Ri*; black), temperature (gray), Thorpe scale (green), nitrate concentration (orange), vertical gradient of nitrate concentration (cyan), vertical diffusivity (blue), and vertical turbulent nitrate flux (red) for (e–g) station M13 and (h–j) station M18. Black dashed lines in (e) and (h) indicate the $Ri = 0.25$ critical value.

A wedge-shaped recirculation flow in the lee of the sill but toward the sill (red vectors in Figures 2a and 2c) can be seen in the horizontal vector plot of the 264 m layer (Figure 1c). Downstream from the point at which the flow direction changed, the mean shear layer shallowed from 300 m at the immediate lee of the sill to 100 m about 5 km downstream. Trains of Kelvin-Helmholtz (KH) billows (thickness = 60 m) were captured as the cat's eye shaped structures by the echogram along the shear layer (Figure 2c). At station M18 (see Figure 1c for the location), one of the billows was observed, with $Ri \ll 0.25$ at 250 m (Figure 2h), indicating flow instability due to shear. In a layer showing a large thermal inversion ($L_T > 10$) between 225 and 275 m, L_T reached 26 m (Figure 2i), ϵ (magenta line in Figure 2h) reached $O(10^{-5}$ W kg$^{-1})$, and K_ρ (blue line in Figure 2j) reached $O(10^{-1}$ m^{2}s$^{-1})$ as a result of KH instability.

The vertical section of ϵ (Figure 2d) shows highly turbulent layers associated with the SBBL above the sill as well as at the KH billows. A remarkably turbulent patch in the surface layer also is evident near the end of the survey (stations M36 to M38; see Figure 1b for the location). This high-turbulence patch was also associated with shear instability, as indicated by the velocity profiles near those stations recording high turbulence (Figure 2a). This patch of enhanced turbulence appeared suddenly 14 km downstream of the sill without visible connection to the upstream instability phenomena. For clarifying the cause of the isolated high-turbulence patch, further investigations are required.

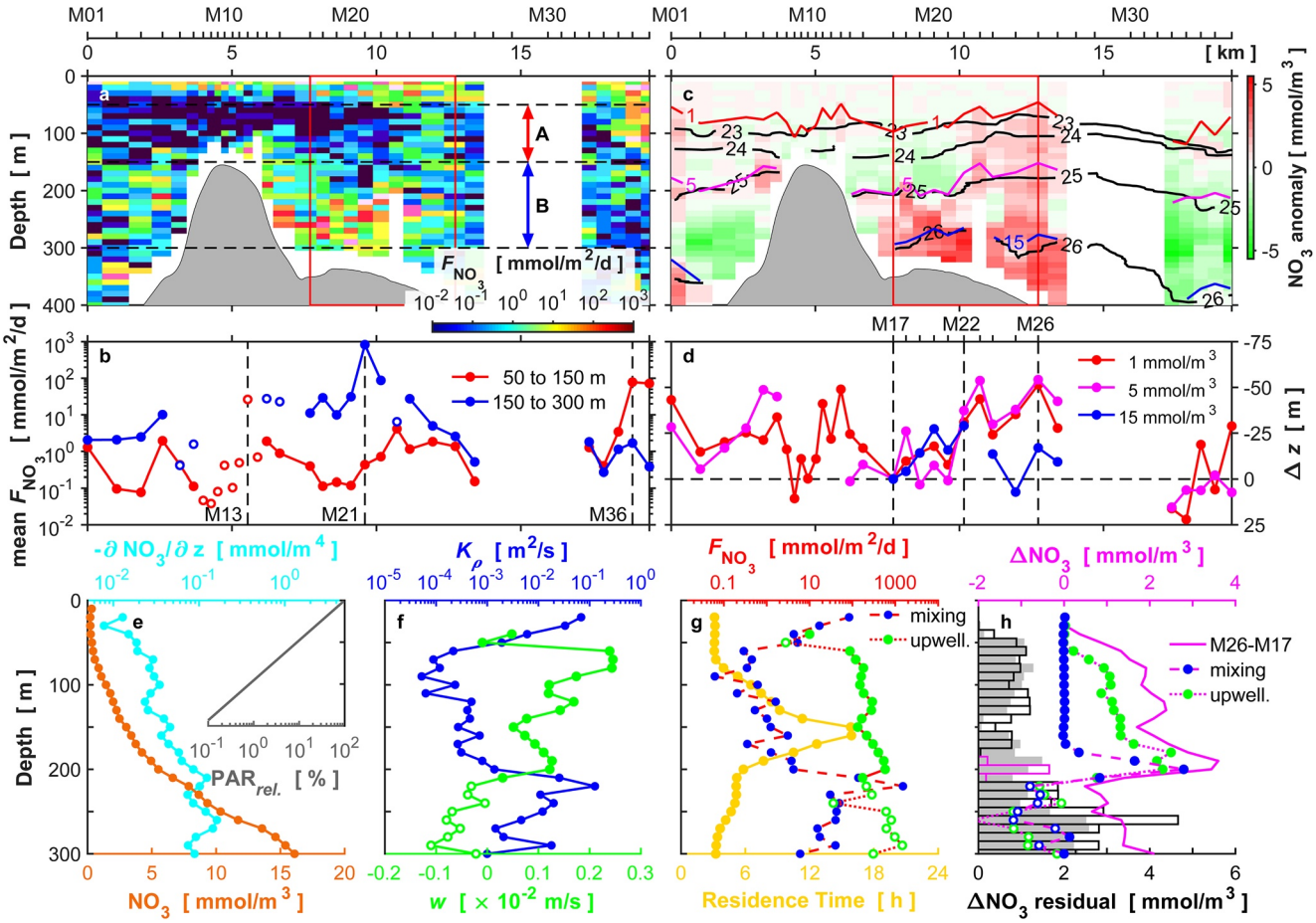

Figure 3. (a) Turbulent vertical nitrate flux during the drifting survey. Nitrate data are missing for stations M28 through M32 due to battery failure. (b) Averaged turbulent vertical nitrate flux in the subsurface layer (red circles; layer marked as A in (a)) and in the intermediate layer (blue circles; layer marked as B in (a)). Open circles indicate stations where the profiling depth did not fully cover the averaging layers. (c) Nitrate concentration anomaly along the drifting survey. Black contours represent isopycnals. Red, magenta, and blue lines indicate 1, 5, and 15 mmol m^{-3} nitrate isolines; corresponding isoline depths for the section are plotted in (d). (e–g) Averaged profiles between stations M17 and M26 (region in red box in (a)) for nitrate concentrations (orange in e), relative irradiance (gray in e), vertical gradient of nitrate concentration (cyan in e), vertical diffusivity (blue in f), vertical velocity estimated based on the change in the density profile (green in f), turbulent vertical nitrate flux (the red dashed line with the blue circles in g), upwelling nitrate flux (the red dotted line with the green circles in g), and residence time (yellow in g). Observed nitrate increase from M17 to M26 (the magenta solid line in h), estimated nitrate increase by the turbulent mixing (the magenta dashed line with the blue circles in h), estimated nitrate increase by the upwelling (the magenta dotted line with the green circles in h), residual part of the nitrate increase which cannot be explained by the sum of the observed turbulent mixing and estimated upwelling (the black-edged bars in h; the magenta-edged bar indicates a negative value), and nitrate increase along the isopycnal surfaces (the gray bars in h). The open circles in figures (f–h) indicate negative values.

3.2. Nitrate Flux

Throughout the drifting survey, the nitrate concentration in the surface layer was depleted below 1 mmol m^{-3} (Figure 3c). At station M13, where the SBBL was evident, the nitrate concentration gradually increased with increasing depth starting at 90 m depth (Figure 2f) with a vertical gradient magnitude of $O(10^{-2}$ mmol m^{-4}; cyan line in Figure 2g). In the subsurface layer below 150 m depth at M18, the vertical gradient steepened to $O(10^{-1}$ mmol m^{-4}; Figure 2j).

In the highly turbulent SBBL, K_ρ reached $O(10^{-1}$ m^2 s$^{-1})$ at 130 m depth at station M13, and the turbulent vertical nitrate flux reached $O(10^2$ mmol m^{-2} day^{-1}; red line in Figure 2g). In the intermediate layer from 150 to 300 m at station M18, the maximum nitrate flux reached $O(10^2$ mmol m^{-2} day$^{-1})$ in the bottom part of the KH billow (Figure 2j). The flux in the upper half of the billow showed a lower value of $O(10^{-1}$ mmol m^{-2} day$^{-1})$ because part of the water column was already mixed.

The vertical section of turbulent nitrate flux (Figure 3a) shows a high-flux band in the layer with the KH billows; this band extended downstream for over 5.0 km between M17 and M26 (red box in Figure 3a). The en-

hanced nitrate flux reached $O(1–10^3$ mmol m^{-2} day$^{-1})$, and the maximum fluxes of $O(10^3$ mmol m^{-2} day$^{-1})$ were located at stations M21 and M22, at 210 and 200 m, respectively. High fluxes of $O(10^2$ mmol m^{-2} day$^{-1})$ were also found in the subsurface layer at stations M36 and M37 where enhanced mixing was observed (Figure 2d). On the other hand, a low-flux band was observed along the surface jet where turbulence was inactive. The observed nitrate flux of $O(10^3$ mmol m^{-2} day$^{-1})$ represents an extremely large turbulent flux value, apparently larger than any reported for the open ocean, but is of the same order as that of an energetic tidal estuary reported by Cyr et al. (2015).

In terms of the direct effect of nutrient flux to the ecosystem, the important flux is that to the layer above the compensation depth, that is the euphotic layer, where net photosynthesis is positive (Cullen, 2015). The compensation depth coincides with the depth where the relative light level, $\mathrm{PAR_{rel.}}(z) = \mathrm{PAR_{water}}(z)/\mathrm{PAR_{surf}} \times 100\%$, is 0.1%–1% (Laws et al., 2014). Here, $\mathrm{PAR_{water}}(z)$ is the vertical profile of the Photosynthetically Active Radiation in the water, and $\mathrm{PAR_{surf.}}$ is the surface radiation. The mean radiation profile based on the mean attenuation coefficient ($\overline{K_d} = -0.048$ m^{-1}) obtained by a PAR sensor during the survey (gray line in Figure 3e) indicates a compensation depth of 143 m for a light level of 0.1%, and a compensation depth of 96 m for a light level of 1%. The enhanced flux did not affect the surface layer, as the shallowest depth observed during the survey for the nutricline defined by a 1 mmol m^{-3} nitrate concentration was 46 m (red line in Figure 3c). The layer-averaged flux for depths from 50 to 150 m (hereafter we call the layer the subsurface layer), corresponding with the lower euphotic layer, shows high values of $O(10$ mmol m^{-2} day$^{-1})$ in the lee of the sill peak (station M13) associated with the SBBL. Values of $O(10^2$ mmol m^{-2} day$^{-1})$ were observed at stations M36 and M37 where an isolated turbulent patch was observed (red circles in Figure 3b). These enhanced fluxes in the euphotic layer are expected to affect the downstream ecosystem.

The nitrate flux associated with KH billows was limited in the layer below the euphotic layer between 150 and 300 m (hereafter, we call the layer as the intermediate layer). The layer-averaged flux for the intermediate layer (blue circles in Figure 3b) was mostly far higher than $O(1$ mmol m^{-2} day$^{-1})$ for the section with the KH billows (stations M17 to M26), and a peak value of $O(10^3$ mmol m^{-2} day$^{-1})$ was reached at station M21. The averaged flux profile of the section (red dashed line with blue circles in Figure 3g) indicates a turbulent layer around the KH billows with a peak $F_{\mathrm{NO_3}}$ value of $\sim O(10^3$ mmol m^{-2} day$^{-1})$ at 220 m.

To evaluate the contribution of the turbulent vertical nitrate flux to the change in nitrate concentration in the water column, we performed a simplified 1D mixing model calculation for the section between stations M17 and M26 as follows:

$$\Delta \mathrm{NO_{3}}_{mix.}(z) = \int_0^{\overline{T_R}} \frac{\partial}{\partial z}\left(\langle K_\rho(z) \rangle \frac{\partial \mathrm{NO_3}(z,t)}{\partial z} \right) dt, \tag{2}$$

where $T_R(z) = L/|u(z)|$ is the layer residence time in the section between stations M17 and M26 (yellow line in Figure 3g), $u(z)$ is the mean horizontal velocity profile, and $L = 5.0$ km is the cumulative distance of the section. For the computational simplicity, a vertically averaged value ($\overline{T_R}$) was used. $\langle K_\rho(z) \rangle$ is the section-averaged turbulent diffusivity profile. A 50 m scale vertical smoothing was applied to $\langle K_\rho(z) \rangle$ to study the overall effect of the turbulent mixing. We used the most upstream profile (M17) of the section as the initial condition. During the calculation, the flux was limited to maintain minimal stratification (i.e., $-\partial \mathrm{NO_3}/\partial z > 0$) in order to prevent the turbulent flux from causing concentration inversions.

The dashed magenta line with blue circles in Figure 3h represents the model result. In the layer between 175 and 215 m, the estimated mixing effect indicates the nitrate increase of 55.9 mmol m^{-2} associated with strong turbulent mixing by the KH billows. However, the increased nitrate is supplied from the layer below the flux peak, so the column-total change for the intermediate layer (150–300 m) is small as +7.0 mmol m^{-2}. The estimated changes due to mixing in the subsurface layer (50–150 m) are generally small, and the total change for this depth range is only +0.2 mmol m^{-2}. On the other hand, the actual change in the nitrate profile for this section (i.e., the increase from station M17 to station M26, plotted as a magenta line in Figure 3h) is positive for depths of 40 m and beyond. The increases in column-total nitrate concentration for the subsurface and intermediate layers are 186.0 and 263.6 mmol m^{-2} respectively. Therefore, mixing effects are almost hidden for the column-total changes. Focusing solely on the KH billow layer, the mixing

contribution to the actual concentration change is 40.1%. Indeed, this mixing contribution can be seen as a maximum peak on the observed profile change around 200 m, where the mixing contribution profile also takes the peak (solid magenta line on Figure 3h).

As above, turbulent mixing can still be an important process in explaining the local increase in nitrate concentration in the intermediate layer, but not in the subsurface nor for the column-total increases for this section. Therefore, other processes must be responsible for explaining the nitrate concentration increases.

The vertical section of nitrate concentration anomaly (Figure 3c) shows domings of the nitrate 1, 5, and 15 mmol m^{-3} isolines downstream from the sill, along with isopycnals of roughly 23, 25, and 26 σ_θ, respectively. Fluctuations in the nitrate isoline depths with respect to the values measured at station M17 (Figure 3d) indicate rises in the isolines along the section from station M17 to station M26. Meanwhile, the column-total concentration for the euphotic layer roughly doubles from 60.0 mmol m^{-2} at station M17 to 131.0 mmol m^{-2} at station M26. The maximum rises for the 1 and 5 mmol m^{-3} isolines at station M26 are 51 and 54 m, respectively. For the 15 mmol m^{-3} isoline, the maximum rise is 29 m at station M22.

As an alternative to vertical mixing, "upwelling" may be responsible for the nitrate concentration increases. The vertical velocity w required for the density change ($\Delta\sigma_\theta$) can be estimated as

$$w(z) \sim \Delta\sigma_\theta(z) / \frac{\partial \sigma_\theta}{\partial z} T_R(z). \tag{3}$$

The estimated w (green line on Figure 3f) reaches a peak value of 0.25×10^{-2} m s^{-1} at 70 m but approaches zero at the surface and at 210 m. At depths deeper than 220 m, w becomes negative. The w profile suggests the existence of a surface divergence layer up to the depth of the vertical velocity peak, as well as a convergence layer below.

The nitrate flux associated with upwelling can be obtained as $F_{NO_{3upwell.}} = w(z)NO_3(z)$. The estimated upwelling flux (dotted red line with green circles in Figure 3g) is larger than the flux due to mixing, except in the surface layer and in the layer containing the mixing flux peak at the KH billow. Below a depth of 210 m, the flux is negative because the direction of the estimated vertical velocity is downward. The mean upwelling flux in the subsurface layer (50–150 m) is 158.2 mmol m^{-2} day^{-1}. This upwelling flux explains 48.3% (89.9 mmol m^{-2}) of the observed nitrate increase in the layer. The black-edged bars in Figure 3h show the residual (unexplained) changes calculated by subtracting the mixing and upwelling contributions from the observed change. The column-total residual nitrate increase in the subsurface layers is 51% (95.9 mmol m^{-2}). Because the effect of the nutricline uplift has been already accounted for as the upwelling contribution, the residual increase could be attributed to changes along the isopycnal surfaces. These changes, occurring between M17 and M26, were analyzed in the density coordinate and then projected back on the depth coordinate using the density-depth relationship at M26 (gray bars in Figure 3h). The column-total change along the isopycnal surfaces is 82.9 mmol m^{-2}, which explains 87% of the residual change. The increase in the concentration along the isopycnal surfaces is generally caused by a diapycnal mixing; however, no sufficiently strong turbulence was observed in the subsurface layer of the monitored section can explain this increase. The increase along the isopycnal surfaces can otherwise be attributed to (1) horizontal dispersion and mixing, (2) data limitation (e.g., errors in the nitrate measurements or missing a strong mixing), or (3) analysis errors such as inaccurate vertical second derivatives and isopycnal projection. Here, we propose (1) as the reason for this phenomenon because the sill depth closer to the reef is shallow; therefore, it is perfectly possible that the strong mixing in the shallow layer near the reef enriches the subsurface nitrate and then the enriched water masses are advected to the observed section with the complicated wake flow.

For the intermediate layer (150–300 m), the nitrate increase along the isopycnal surfaces is dominant (216.7 mmol m^{-2}), which explains 82.1% of the total change in this layer, whereas the upwelling contribution is 40.2 mmol m^{-2} (15.2%). Even though the mixing contribution is large in the KH billow layer, the column-total contribution of the mixing is small (7.1 mmol m^{-2}) and cannot explain the large increase along the isopycnal surfaces. Thus, here too, horizontal processes were suggested as the reason for the nitrate increase in the intermediate layer.

4. Conclusions

The flow of the Kuroshio past a shallow sill on the flank of Hira-se is actively turbulent and exhibits bottom boundary layer separation, and Kelvin-Helmholtz instability. These processes produce patches of turbulent nitrate flux that are extremely strong for the open ocean. In addition, the observed nitracline rise with isopycnal doming suggests strong upwelling in the lee of the reef. The magnitude of the estimated upwelling nitrate flux is one order smaller than the peak value of the turbulent nitrate flux but encompasses the entire subsurface layer. The combination of mixing and the upwelling cultivates the water column and results in significant nutrient enrichment in the euphotic layer. Nevertheless, the observed turbulent flux and estimated upwelling cannot explain the total change in the nitrate profile. The large nitrate increase along the isopycnal surfaces suggested the occurrence of horizontal processes; though the enriched water is probably being originally introduced by the turbulent mixing near the reef.

Since the Kuroshio Current always passes through ridges with abrupt topographies, we expect constant existences of vigorous turbulent mixing, strong upwelling, and strong vertical and horizontal nutrient fluxes in those regions. Therefore, considerable efforts are still required for fully grasping the total effects of these flow-topography interactions on the Kuroshio Current and its ecosystem.

Data Availability Statement

The in situ observational data that support the findings of this study are openly available at http://dx.doi.org/10.17632/nx8tz6gcw2.1. The Ssalto/Duacs altimeter products are produced and distributed by the Copernicus Marine and Environment Monitoring Service (CMEMS) (https://marine.copernicus.eu).

Acknowledgments
The authors thank the captain, crew, and students of the TRV *Kagoshima Maru* for time and help. We are grateful to the two reviewers for their useful comments and suggestions that led to considerable improvement of the paper. The field program was conducted as a part of the OMIX project (MEXT KAKENHI Grant Number JP15H05818, JP15H05821, JP18H04914, JP16H01590, and JP18H04920). We also thank Dr. I. Yasuda for his great leadership on the OMIX project.

References

Chang, M.-H., Jan, S., Liu, C.-L., Cheng, Y.-H., & Mensah, V. (2019). Observations of island wakes at high Rossby numbers: Evolution of submesoscale vortices and free shear layers. *Journal of Physical Oceanography*, *49*(11), 2997–3016. https://doi.org/10.1175/JPO-D-19-0035.1

Chang, M.-H., Jheng, S.-Y., & Lien, R.-C. (2016). Trains of large Kelvin-Helmholtz billows observed in the Kuroshio above a seamount. *Geophysical Research Letters*, *43*(16), 8654–8661. https://doi.org/10.1002/2016GL069462

Chang, M.-H., Tang, T. Y., Ho, C.-R., & Chao, S.-Y. (2013). Kuroshio-induced wake in the lee of green island off Taiwan. *Journal of Geophysical Research: Oceans*, *118*(3), 1508–1519. https://doi.org/10.1002/jgrc.20151

Cullen, J. J. (2015). Subsurface chlorophyll maximum layers: Enduring enigma or mystery solved? *The Annual Review of Marine Science*, *7*, 207–239. https://doi.org/10.1146/annurev-marine-010213-135111

Cyr, F., Bourgault, D., Galbraith, P. S., & Gosselin, M. (2015). Turbulent nitrate fluxes in the lower St. Lawrence estuary, Canada. *Journal of Geophysical Research: Oceans*, *120*(3), 2308–2330. https://doi.org/10.1002/2014JC010272

Doty, M. S., & Oguri, M. (1956). The island mass effect. *ICES Journal of Marine Science*, *22*(1), 33–37. https://doi.org/10.1093/icesjms/22.1.33

Furuya, K., Takahashi, M., & Nemoto, T. (1986). Summer phytoplankton community structure and growth in a regional upwelling area off Hachijo Island, Japan. *Journal of Experimental Marine Biology and Ecology*, *96*(1), 43–55. https://doi.org/10.1016/0022-0981(86)90012-2

Guo, X. Y., Zhu, X.-H., Long, Y., & Huang, D. J. (2013). Spatial variations in the Kuroshio nutrient transport from the East China Sea to south of Japan. *Biogeosciences*, *10*(10), 6403–6417. https://doi.org/10.5194/bg-10-6403-2013

Hasegawa, D. (2019). Island mass effect. In T. Nagai, H. Saito, K. Suzuki, & M. Takahashi (Eds.) *Kuroshio current* (pp. 163–174). American Geophysical Union (AGU). https://doi.org/10.1002/9781119428428.ch10

Hasegawa, D., Tanaka, T., Matsuno, T., Senjyu, T., Tsutsumi, E., Nakamura, H., et al. (2019). Measuring the vertical turbulent nitrate flux using sensors. *Bulletin on Coastal Oceanography*, *57*(1), 59–64. https://doi.org/10.32142/engankaiyo.2019.8.008

Hasegawa, D., Yamazaki, H., Ishimaru, T., Nagashima, H., & Koike, Y. (2008). Apparent phytoplankton bloom due to island mass effect. *Journal of Marine Systems*, *69*, 238–246. https://doi.org/10.1016/j.jmarsys.2006.04.019

Hasegawa, D., Yamazaki, H., Lueck, R. G., & Seuront, L. (2004). How islands stir and fertilize the upper ocean. *Geophysical Research Letters*, *31*(16). https://doi.org/10.1029/2004GL020143

Hsu, P.-C., Chang, M.-H., Lin, C.-C., Huang, S.-J., & Ho, C.-R. (2017). Investigation of the island-induced ocean vortex train of the Kuroshio current using satellite imagery. *Remote Sensing of Environment*, *193*, 54–64. https://doi.org/10.1016/j.rse.2017.02.025

Kobari, T., Honma, T., Hasegawa, D., Yoshie, N., Tsutsumi, E., Matsuno, T., et al. (2020). Phytoplankton growth and consumption by microzooplankton stimulated by turbulent nitrate flux suggest rapid trophic transfer in the oligotrophic Kuroshio. *Biogeosciences*, *17*(9), 2441–2452. https://doi.org/10.5194/bg-17-2441-2020

Laws, E. A., Letelier, R. M., & Karl, D. M. (2014). Estimating the compensation irradiance in the ocean: The importance of accounting for non-photosynthetic uptake of inorganic carbon. *Deep Sea Research Part I: Oceanographic Research Papers*, *93*, 35–40. https://doi.org/10.1016/j.dsr.2014.07.011

Nagai, T., Durán, G. S., Otero, D. A., Mori, Y., Yoshie, N., Ohgi, K., et al. (2019). How the Kuroshio Current delivers nutrients to sunlit layers on the continental shelves with aid of near-inertial waves and turbulence. *Geophysical Research Letters*, *46*(12), 6726–6735. https://doi.org/10.1029/2019GL082680

Nagai, T., Hasegawa, D., Tanaka, T., Nakamura, H., Tsutsumi, E., Inoue, R., & Yamashiro, T. (2017). First evidence of coherent bands of strong turbulent layers associated with high-wavenumber internal-wave shear in the upstream Kuroshio. *Scientific Reports*, *7*(1), 14555. https://doi.org/10.1038/s41598-017-15167-1

Osborn, T. R. (1980). Estimates of the local rate of vertical diffusion from dissipation measurements. *Journal of Physical Oceanography*, *10*(1), 83–89. https://doi.org/10.1175/1520-0485(1980)010<0083:eotlro>2.0.co;2

Tanaka, T., Hasegawa, D., Yasuda, I., Tsuji, H., Fujio, S., Goto, Y., & Nishioka, J. (2019). Enhanced vertical turbulent nitrate flux in the Kuroshio across the Izu ridge. *Journal of Oceanography*, *75*(2), 195–203. https://doi.org/10.1007/s10872-018-0500-2

Tsutsumi, E., Matsuno, T., Lien, R.-C., Nakamura, H., Senjyu, T., & Guo, X. (2017). Turbulent mixing within the Kuroshio in the Tokara strait. *Journal of Geophysical Research: Oceans*, *122*(9), 7082–7094. https://doi.org/10.1002/2017JC013049

Uda, M., & Ishino, M. (1958). Enrichment pattern resulting from eddy systems in relation to fishing grounds. *Journal of the Tokyo University of Fisheries*, *44*(12), 105–129.